



Effect of Annealing Temperature on Microstructure, Mechanical Properties and Penetration of Shear Formed C10100 Copper Shaped Charge Liners



CrossMark

T. Elshenawy^{1,*}, Ahmed Abd Elhady², A. M. Riad², Mohamed Abd Elkader²

¹ Technical Research Centre, Cairo, Egypt

² Military Technical College, Egyptian Armed Forces, Kobry Elkobbah, 11765, Egypt

*E-mail: tamershenawy@yahoo.com

<https://orcid.org/0000-0002-9934-9178>

Abstract

The influence of annealing temperature on mechanical properties of C10100 copper when used as a shaped charge liner has been investigated. The cold worked liners manufactured by spinning technique are annealed at temperatures 200 to 600 oC to obtain grain sizes 10.6 to 49.4 μm . The Zerilli-Armstrong model is used to calculate the necking strain and the velocity difference between jet fragments (V_{PL}) using Kolsky approach for copper with grain sizes from 10.6 to 49.4 μm ; which were found 96.1 and 99.7m/s; respectively. Besides, Autodyn has been implemented to estimate the jet velocity, temperature and its penetration into 1006 steel targets. The effect of the liner grain size has also been confirmed by the static firing of these shaped charges including liners with different grain sizes after filling with waxed HMX. Results showed that the measured penetration depths increase from 12.63 to 13.77cm into 1006 steel targets when the yield strength of the copper liners increases from 69 to 95 MPa; respectively. This effect was accounted by incorporating the liner yield strength values within the well-known Allison-Vitalli formula, which accounts for this variation in the penetration tests when liners with different grain sizes and different yield strengths are tested and regarded.

"Keywords: Copper C10100; annealing temperature; shaped charge, liner yield strength, grain size, penetration."

1. Introduction

Researchers have shown an increased interest in the different liner materials and their manufacturing techniques. Copper material has many applications because of its optimum properties such as high ductility, malleability, high corrosion resistance, easiness of manufacturing and abnormal electrical and thermal conductivity levels. Heat treatment for copper and its alloys is necessary during the manufacturing process. Such heat treatment has a noticeable effect on the microstructure and grain size of the resultant copper liner [1], which in turn has a major effect on the jet ductility and its penetration potential into target materials when used as a shaped charge liner. Various research work has been conducted to assess the potential of these shaped charge copper liners having various average grain sizes and related microstructure. Elshenawy [2] analytically studied the breakup time and the relevant total number of fragments over a wide range of copper liner with grain size ranging from 0.5

to 100 μm over different jet temperatures for small caliber liners produced by the electrodeposition technique. The average copper grain sizes produced by this technique were determined by scanning electron microscopy (SEM) and found to be 1 to 5 μm . In this study, the Zerelli Armstrong constitutive model [3] was selected to estimate the plastic particle velocity or the velocity difference between jet fragments (V_{PL}), which is related directly to breakup time of the jet. The results showed that electrolytic copper liners with fine grain sizes showed lower (V_{PL}) values and thus longer break-up times than those with coarse grain sizes. Besides, the predicted number of fragments were found to increase with decreasing the grain size too.

Petit et al [4] has performed experimental analysis on the breakup of copper shaped-charge jets using X-ray diagnostic technique in addition to numerical study using OURONAOS. Additionally, a combined numerical and analytical analysis is devoted to analyze the jet break-up time of a shaped-charges of 62 mm diameter and 48 degree conical copper liners.

*Corresponding author e-mail: tamershenawy@yahoo.com; (Tamer Elshenawy).

Receive Date: 25 January 2023, Revise Date: 04 April 2023, Accept Date: 11 April 2023

DOI: 10.21608/EJCHEM.2023.178816.7268

©2023 National Information and Documentation Center (NIDOC)

The copper grain size ranging from 20 μm to 130 μm has been used. It was found that reducing the grain size from 130 μm to 10 μm increases the flow stresses of copper nearly by 20 MPa in the jet material and hence, increases the cumulative jet length of the used shaped charge.

Ridhwan et al. [5] studied the effect of both the heat treatment and relevant cooling rate of C102 copper alloy on relevant microstructure and related mechanical properties. Heat treatment was applied at temperatures; 350, 400, and 450°C for one hour and cooled through two mediums; furnace and water quenching. They found that quenched specimens underwent high cooling rate exhibits higher strength than that of annealed ones due to local strain effect. They also found that with increasing the temperature for annealing specimens there is a grain growth occurs due to the generated pinning particles and associated dissolution of from the grain boundary. In addition, quenched samples showed finer grains due to heat treatment because of the grain clustering effect.

Edwards et al [6] examined the penetration behavior of 99.9 % copper EFPs in order to determine the effect of the initial liner microstructure using two series 1.2mm and 4mm liner wall thicknesses of different heat treatments. The firing is done against 3 different types of steel targets, Type A: 25mm thick steel (hardens 123 Vickers), Type B: 25mm thick steel (hardens 133 Vickers), Type C: 10mm thick steel (hardens 142 Vickers). The resulted penetration was measured and found to vary according to the obtained grain size and the used thickness of copper liners. It was shown that at 200°C annealing temperature, which produces a fine grained micro structure, the penetration was recorded the best result as shown in [6] due to the fine microstructure and expected most ductile EFP.

OFHC (4N purity) has been tested dynamically using stainless steel flyer plate of 4.7mm thickness accelerated by PBX 9501 explosive. The impact velocity of the accelerated steel plate of thickness 4.7mm was 2200m/s [7]. The fine grain material was found to exhibit abnormal enhanced potential due to the retarded localization, which results in increased break-up time and larger penetration depth as expected.

Among grain size, overall impurity content and total ductility of liner parameters, Schwartz et al [8] applied geometrical analysis to conclude the governing relationship among these parameters in a shaped charge copper liners of base inner diameter 81 mm and apex angle 42 degree. After the cold forging to produce liners, they have been annealed at 315 °C for 1 hour to prevent sulfur doping. The microscopic examination of the grain size revealed that liners with

smaller grain size and less sulfur content have a longer break up time [8].

Agu et al [9] tested liners manufactured by both machining and the additive manufacturing using selective laser sintering process. These liners have been driven by explosive loading to form shaped charge jet and slug. The used liner design has charge diameter of 50mm with liner wall thickness of 1.5 mm and cone angle of 42°. The optical and scanning electron microscope examination of the liners and resultant slugs have been performed using these techniques. It was concluded that both liner produced by these two processing techniques showed fine elongated grain sizes for the recovered slug due to the dynamic recrystallization, which may be indication for enhanced predicted jet penetration.

Tian et al. [10] applied the electroforming technique to produce conical copper liners of shaped charges of diameters 105 mm and thickness of 2mm. Analysis of plastically deformed microstructures has been conducted by Transmission electron microscopy (TEM), SEM, and optical microscopy at different strain rates. They found that changes of the liner microstructure and the dynamic behaviour of liner material have significant effect on the produced recovered slug material when ultra-strain rate as much as 10 s⁻¹ is applied.

Based on the presented discussions including the effect of copper liner grain size on the shaped charge penetration potential into different targets, it was found that copper liner grain size has a tremendous effect that cannot be neglected and should be considered within hydrodynamic penetration models. The effect of the jet yield strength on the later stages of hydrodynamic penetration has been addressed by Eichelberger [11, 12], who added two strength terms to the hydrodynamic equations to account for their influences on the penetration in the latter stage of penetration according to the formula:

$$\lambda \rho_j (V - U)^2 = \rho_T U^2 + 2\sigma \quad (1)$$

Where, U is the penetration velocity, ρ_T and ρ_j are the target and jet densities respectively, V is the jet velocity. $\sigma = \sigma_T - \sigma_j$, in which σ_T and σ_j are the resistance to plastic deformation for the target and jet respectively. These terms of strength are taken as one to three times the static uniaxial yield stress (σ_y). λ in Eq. (1) should be lower than unity when the jet is broken. Unfortunately, this equation cannot be used directly because it brings one more unknown parameter, which is the penetration velocity; U. To carry on with an explicit function containing only one unknown, many trials have been introduced and justified. The influence of target material strength on the jet penetration during the hydrodynamic regime has also been investigated by introducing a correction

term depending on the target strength in the hydrodynamic formula [13], i.e.

$$P = \sqrt{\frac{\rho_j}{\rho_T}} L \left(1 - \frac{\alpha Y}{\rho_j V^2} \right) \quad (2)$$

Where, α is a constant; L is the length of the rod penetrator; Y is the dynamic yield strength of the target; V is the velocity of the penetrator at impact. The correction term was related somehow to the well-known non-dimensional number in impact dynamics known as Johnson's damage number [14, 15], which accounts for penetration reduction due to the dynamic yield strength of the target. This approach is limited to the long rod penetrator and cannot be used with variable velocity shaped charge jet. Alternatively, the modified Allison and Vitalli model [16], which deals with velocity gradient jet has been used to account for the penetration reduction of an oil well perforator into concrete targets under its compressive strength and the hydrostatic confinement [17]. Elshenawy and Li [17] studied this effect by incorporating correction term into the Allison-Vitali equation for a continuous jet, i.e.

$$P = Z \left[\left(\frac{V_j}{V_c} \right)^{\frac{1}{\gamma}} - 1 \right] \left(1 - \frac{\lambda f_c'}{\rho_j V_c^2} \right) \quad (3)$$

Where, Z_0 is the effective jet length between the virtual origin (VO) point to the target surface; V_0 and V_c are the jet tip and cut-off velocity, respectively; γ is the square root of the target-jet density ratio (i.e. $\gamma = \sqrt{\rho_T / \rho_j}$). f_c' is the compression strength of concrete, which represents great dependence on the applied hydrostatic pressure [18, 19]; λ is a constant that can be estimated from real experiments. This constant was found to be 200.31, which showed satisfactory agreement with experimental results.

Allison & Vitalli formula [16] was also modified [20] by introducing a target resistance reduction term, which accounts for target resistance to penetration based on Wright and Frank analysis method [21] and Rosenberg and Dekel [22];

$$P = \left(\frac{(Y+1)(V_0 t_b)^{\frac{1}{\gamma+1}} Z_0^{\frac{\gamma}{\gamma+1}} - V_c t_b}{\gamma} - Z_0 \right) \left(1 - \lambda \frac{R_t}{\rho_j V_c^2} \right) \quad (4)$$

For $V_c t_b \left(\frac{V_c}{V_0} \right)^{\frac{1}{\gamma}} \leq Z_0 < V_0 t_b$, in which the jet break-up happens during penetration.

Where, t_b is the jet break-up time and R_t is the target resistance to plastic deformation and defined by; $R_t = A Y_t \left(1 + B \ln \frac{2E}{3Y_t} \right)$, (5)

E is the Young's modulus and Y_t is the target yield strength. A and B are constants that have been optimized and found to be 0.5 and 0.73; respectively.

λ is constant, which represents a dependence on the target yield strength according to:

$$\lambda = 0.8322 Y_t + 0.6122 \quad (6)$$

This constant shows significant dependence on the cut-off velocity in addition to the target yield strength when the cut-off velocity is greater than 3 km/s [20, 23].

Unfortunately, Eq. (4) cannot be used directly because it does not consider the mechanical properties of the liner material when its grain size is regarded and more than one grain size liner is tested. The development to penetration equation other than Eq. (4) is necessary to include the effect of the liner yield strength and its significance on the penetration enhancement.

Based on the presented discussions including the effect of grain size on the mechanical properties of C10100 copper grade and its impact on the jet ductility, calculated jet tip velocity as well as its penetration potential, the current research is devoted to analyse these parameters numerically and analytically for the C10100 copper liners manufactured by flow forming techniques. The complete analysis of the penetration variation is presented in this paper using necessary analysis, where various shaped charges with liners having different grain sizes have been used to obtain different jet tip and cut-off velocities to validate the proposed reduction term and related modification. This impact is emphasized by the static firing of copper liners with different grain sizes against steel 1006 laminated target.

Section 2 in this research describes the experimental set-up and configurations of the shaped charge. *Section 3* introduces the numerical and material models and material parameters used to simulate the shaped charge jet and its penetration. Results will be discussed in *Section 4* with detailed analysis including the jet temperature estimation, the characteristic plastic particle velocity (the velocity difference between two neighbouring jet fragments), and eventually, the breakup time, which is followed by conclusions to the penetration testing in *Section 5*.

2. Experimental Work

2.1. Materials and Methods

The explosive charge load used within the current research is Octocire containing 96% HMX and 4% Wax obtained from Euroenco, France.

The manufacturing technique applied in the current research, which is implemented to produce the copper liner is the spinning (shear forming) process. In this technique softened sheet of C10100 copper is deformed against the mandrel shape that determines the inner shape of the liner. After this stage final

process by which excess material will be machined off to remove excess copper material. Stress-relive heat treatment cycle is applied to the produced liners to remove the work hardening related to cold working. The predicted equi-axed grains of the produced copper liner would be less than 30 μm [24]. A schematic drawing of the spinning process is shown in Figure 1.

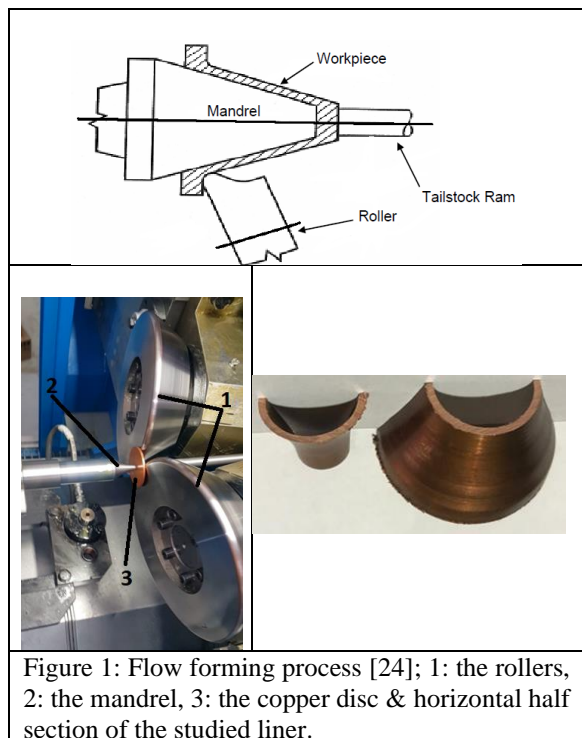


Figure 1: Flow forming process [24]; 1: the rollers, 2: the mandrel, 3: the copper disc & horizontal half section of the studied liner.

2.2. Sample Preparation and Heat Treatment

The high-purity oxygen free electronic copper C10100 (99.99% Cu) is cut out from a sheet at a shape of discs with thickness of 3 mm and 40 mm diameter. After this, the copper is heat treated at 400°C for 60 min and then quenched in water (before cold working) to withstand the forming process without cracking. The heat treated discs are then formed into a liner shape on the shear forming machine. After forming to the final liner shape, the liners are heat treated at different temperatures in the vacuum furnace to study the effect of heating conditions on the resultant grain size and related microstructures. The heat treated liners are then cut and prepared as metallographic specimens. The annealing temperatures were performed at 200, 250, 300, 350, 400, 450, 500, 550 and 600 °C for 30 minutes.

Figure 1 showed half sections of the liner used to study the microstructure and metallographic shape According to ASTM E3 standard [25]. The main steps of the sample preparation are briefly discussed herein. Cutting of the selected specimen from the produced liner, where sample overheating should be avoided using a suitable coolant then, mounting (molding) it in

a thermo-softening plastic e.g. acrylic resin disks with standard dimensions using hot molding machine (about 150°C) for safer handling and easier fixation. Grinding is needed to obtain flat surface using automatic grinding & polishing machine with grades 240 to the very fine emery papers with grades 1500 and 4000. Polishing is then applied to obtain a scratch free surface (mirror like surface) by using automatic grinding & polishing machine using a billiard cloth saturated with an abrasive material (diamond suspension) with three grades (9, 3 and 1 μm). After that washing the mold is performed with a stream of worm water and drying using a hand blower. Etching is the most important step, in which a chemical etchant (distilled water or ethanol (100:120) ml, hydrochloric acid (25:50) ml, ferric chloride (5:10) gram is used to interact with the existing phases and grain boundaries with different severities to increase the contrast. Over etching of the copper specimen should be avoided to reduce the chemical attack phenomena for long time etching, which generate pits that can grow and obscure the main microstructure feature. After all these steps, samples imaging is performed using the optical and Scanning Electro Microscope (SEM) techniques.

2.3. Microstructure Investigation and Average Grain Size Measuring

The mean linear intercept method (M.L.I.) for measuring the grain size in polycrystalline metals and alloys was applied according to ASTM E112 [26]. Using the image j software, the M.L.I. is approximated by counting the total number of the grain boundaries or grains, which intercept a linear traverse of length L. Then, the average grain size d can be estimated by:

$$d = \frac{n \times L \times 10^3}{Z \times N} \quad (7)$$

Where, d is the average grain diameter, n is the number of lines, L is the line length and Z is the total number of grains on the line. Z is the number of grain boundaries intersected and can be estimated when a random line is drawn of known length, then the number of grain boundary intersects (Z) are then counted. Then, Z=1 if the test line is tangential to a grain boundary and Z=1.5 if the test line intersects and triple point. N is the microscope magnification.

2.4. The Micro Hardness and Mechanical Properties Measurements

To investigate hardness of the studied copper specimen, 15 points on the outer copper specimen surface in addition to 10 points through the thickness will be selected. The hardness of each specimen is measured by taking the average of three successive hardness measurements using the 200 gf micro-hardness Vickers hardness test. copper specimens have been prepared according to ASTM E8M [27] along both the transverse (TGD) and the groove direction (GD). The Yield and ultimate tensile strengths, and elongation were also evaluated by the

uniaxial tensile test using universal computerized Electro-500 kN MTS tensile machine according to the standard [28].

3. Numerical Simulation:

3.1. General

The numerical simulation in this paper was conducted using AUTODYN hydro-code software. Two different numerical approaches have been used within the current work, which are the jet formation and jet interaction (penetration) with the used steel targets. The built in standard jetting analysis depending on the unsteady state PER assumption [29] was only implemented when evaluating the preliminary design of the used shaped charge and used for further analytical estimations such as jet radius and breakup time, but it will not be discussed in the current research, however, interested reader can find more detailed data about this jetting algorithm in Ref. [17]. The jet formation is needed to obtain the jet profile using Euler solver at different times from the detonation moment. The Euler solver output is the stretching jet that includes certain velocity which can be used directly as the input of Lagrange-Lagrange jet-target interaction problem. Also the jet contours such as velocity, pressure and many other jet parameters can be shown using this scheme. The second scheme is the penetration of the remapped jet with the steel target, which is modeled using Lagrange method.

3.2. Material Models:

The Jones-Wilkins-Lee (JWL) equation of state is applied to the used high explosive material charge. The density is 1.891 g/cm³, Parameter A=7.782×10⁸kPa, whereas parameter B=7.071×10⁶kPa. r₁=4.2 and r₂= 1. The detonation velocity equals 9100 m/s, while the detonation pressure is 4.2×10⁷ kPa and the C-J Energy per unit volume is 1.05×10⁷ kJ/m³.

The density of the copper liner material is 8.93 g/cm³ with linear EOS with bulk modulus of 1.29×10⁸kPa at reference temperature of 300 K. The strength model is Zerilli-Armstrong(Z-A) constitutive model [3].The Zerilli-Armstrong strength model describes the relation among the deviatoric flow stresses (σ), plastic strain (ϵ), and strain-rate ($\dot{\epsilon}$), temperature (T) and grain size (d) according to the formula:

$$\sigma = C_1 \epsilon^n e^{(-C_2 T + C_3 T \ln \dot{\epsilon})} + C_4 + C_5 d^{-0.5} + C_6 \epsilon^m \quad (8)$$

Where, parameters C₁, C₂, C₃, C₄, C₅, C₆, m and n are constants, d is the average grain size (mm) and $\dot{\epsilon}$ is the strain-rate in (s⁻¹). The model is used to well describe the three effects, which are strain hardening, thermal softening and strain rate effect in

addition to the grain size effect [3].The copper liner material, which is used for our study has a different yield strength that varies from (69:95) MPa with a relevant grain size ranging from (10:49) μm based on measured stress-strain using uniaxial hydraulic press and also in accordance with Hall-Pitch relation [30]. Shear Modulus=4.6×10⁷ kPa; Ref. Strain Rate 1 s⁻¹; C₁=890 MPa; C₂= 0.0028 K⁻¹; C₃=0.000115 K⁻¹; C₄=46.5 MPa; C₅= 5 MPa.mm^{0.5}; n =0.5; Ref.[3, 31].

The charge case was manufactured using steel 4340 with density 7.83 g/cm³, where the linear EOS was applied to account for the detonation high pressure. The bulk modulus is 1.59×10⁸ and the specific heat of 477 J/kg. K are implemented. Thus, the Johnson Cook strength model was applied to simulate the casing under the explosion extreme loading. The shear modulus of this steel is 8.18×10⁷ kPa, yield strength of 7.92×10⁵ kPa and unity reference strain rate.

The steel 1006 target material has a density of 7.896 g/cm³ and shock EOS of Gruneisen coefficient 2.17 and parameter C₁ = 4569 m/s and S₁ = 1.49. The strength model used with the Steel target is Johnson-Cook criteria of shear modulus 8.18×10⁷ kPa, and yield strength of 3.5×10⁵ kPa.

4. Results and Discussion

4.1. Hardness Investigation

Indentation size, which is observed in a soft materials like C10100 Copper can be used as a hardness scale, where it is found that the apparent hardness of this soft material increases as the size of the indent decreases. The goal of the micro hardness measurement is to provide data on the size dependence of hardness measurements for all the tested copper grades; fully annealed, partially and fully work-hardened based on the annealing temperature and its duration (when time is considered within another parametric study).Figure 2 shows the micro hardness test results for the samples of copper specimens annealed at 500°C, 550°C and 600°C for 30 minutes, respectively; for instance.

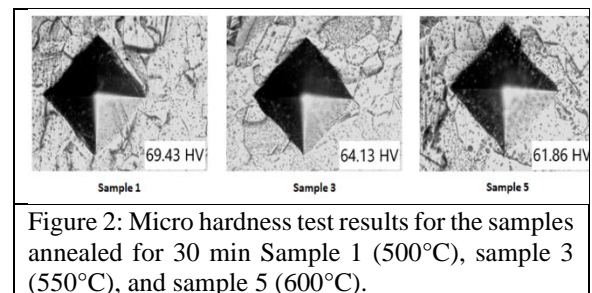


Figure 2: Micro hardness test results for the samples annealed for 30 min Sample 1 (500°C), sample 3 (550°C), and sample 5 (600°C).

Investigation for the hardness-annealing temperature dependence indicates that the increase in

the annealing heat treatment temperature decreases the hardness as correlated in Eq. (9). This inverse relation is described by a simple empirical equation based on the presented best fit linear equation with an error less than 0.01%, this equation is represented by:

$$HV = -0.0493t_{annealing} + 91.615 \quad (9)$$

Where, HV is the Vickers's hardness number and $t_{annealing}$ is the annealing temperature of the copper in Celsius.

4.2. Microstructure Investigation and Grain Size Determination

The microstructure of annealed copper specimens and the average grain size are investigated using both SEM and optical microscopes. Figure 3 shows the micro structure of the copper samples annealed at different temperatures for 30minutes for the horizontal plane section. The presented pictures shows that annealed copper undergo grain coarsening (growth) as the annealed temperature increases from 600° to 200°C. This may be attributed to the reduction of dislocation and the grain growth phenomenon caused by decreasing of the surface energy. This is confirmed by the reduction in the ultimate strength of the annealed copper specimens as shown in Table 1. For the first impression, in accordance with the preferred smaller average copper grain size for better jet dynamic ductility and larger effective jet length [31], the annealing temperature is thought to be as small as possible according to Figure 3, but this is not the fact. The reason behind this is the residual stresses that should be removed before the copper is used as a shaped charge liner. The residual stresses is of great importance so that they should be considered and avoided to guarantees better ductility and larger penetration depth. However, the residual stresses issue will not be discussed herein.

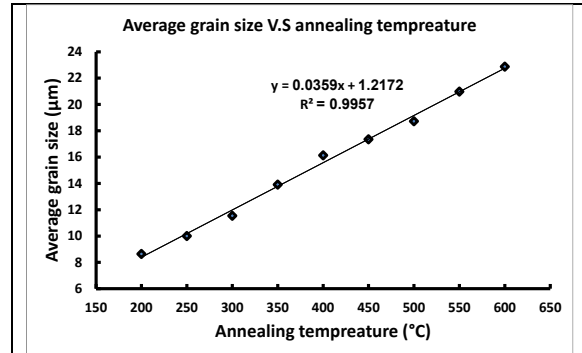
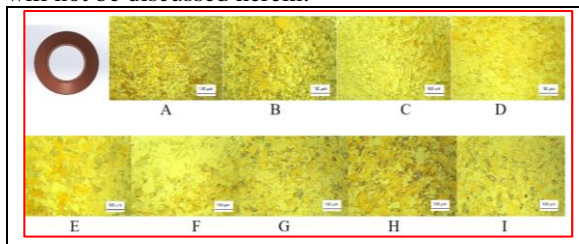


Figure 3: SEM pictures for liners annealed at different temperatures (TOP) and average grain size of the samples vs. annealing temperature at 30 minutes (bottom).

Besides, the grain growth of the annealed copper liner depending on the annealing temperature at 30 minutes undergo the following equation based on empirical best fit finding in Figure 3 as follow:

$$d_{average} = 0.0359t_{annealing} + 1.217 \quad (10)$$

Where, $d_{average}$ is the average grain size of the copper liner and $t_{annealing}$ is the annealing temperature of the copper in Celsius.

Figure 4 shows both the standard tensile test dog bone specimen annealed before applying quasi-static tensile testing using MTS tensile test apparatus, for which stress strain relations are shown in the same figure and summarized in Table 1.

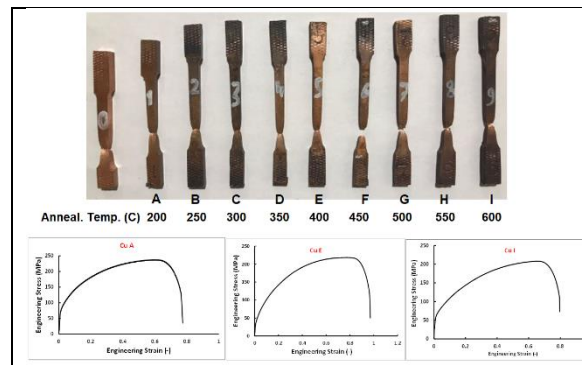


Figure 4: Dogbones tensile test specimen (up) and Stress-strain curves for the copper liners annealed at 200°, 400° and 600° C respectively (bottom).

4.3. Jet Formation

The jet formation is performed using Euler solver based on continuum mechanics to obtain the jet velocities at different stand-off distances when the yield strength of the copper liner material is considered. To do this, fixed gauges have been assigned to measure the jet velocity at different positions as shown in Figure 5 as soon as the jet pass

through them. The maximum velocity readings of these gauges obtained are assembled and shown in the same figure.

Theoretically, the jet deceleration in air is neglected when void replaces the air material within the hydrocode; but data obtained from Figure 5 show different attitude for the same tested yield strength liner although the average decrease in the jet tip velocity is about 152m/s with an average percent of 1.8% for the six liners. It can then be noticed that the yield strength, which increases with decreasing the average grain size of the copper liner is inversely proportional to the jet velocity. This phenomena was also addressed and confirmed by Agu [32] who used three yield strength values of 60, 75 and 90MPa for copper liners and found similar dependence of jet tip velocity on the copper liner yield strength. This relation may not be considered within the unsteady state PER theory, which considers the collapse velocity as a function of Gurney velocity, explosive to metal mass ratio and the geometry type only. Thus, in the classical Gurney models, the mechanical properties of the liner material was ignored with respect to the huge detonation pressure of the applied explosive charge, which exceeded the material strength. On the other hand, in numerical simulations, the mass, momentum and energy are predicted precisely inside each cell considering the liner strength, which in turn reflects the difference in the collapse and jet velocities of each copper liner within a certain yield strength value. These results show the importance of considering the yield strength of the copper liner, which depends mainly on the average grain size of the copper liner material as shown in Hall-pitch and ZA strength models [31].

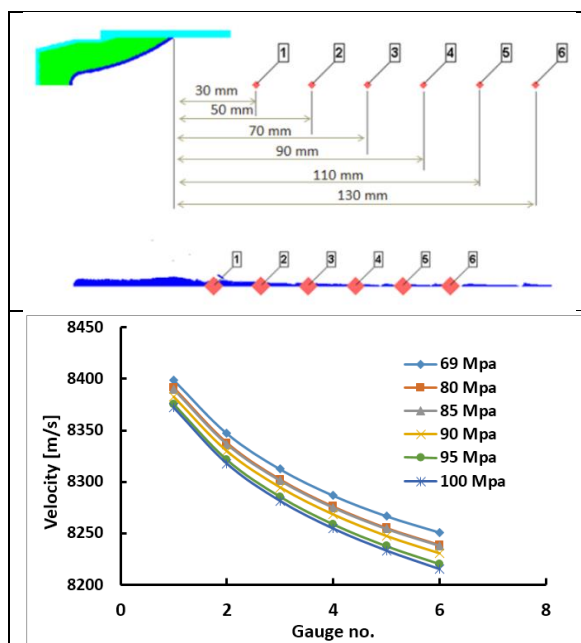


Figure 5: The location of the used gauges to measure the jet velocity at different standoff distances and comparison of the jet velocity at the same positions at different yield strength of the copper liner materials.

4.4. Jet Breakup Time

The breakup time t_b is crucial when determining the shaped charge jet penetration capability into the steel target using analytical models. It was calculated from Hirsh [33], who estimated the breakup time of a jet element according to:

$$t_b = \frac{2r}{V_{PL}} \quad (11)$$

Where, r is the initial radius of the jet element when the jet forms, which can be estimated analytically from:

$$r = \sqrt{2RT_L} \sin\left(\frac{\beta}{2}\right) \quad (12)$$

in which R is the initial inner radius of the liner element and β is the elemental collapse angle of the liner element calculated from jetting analysis based on Pugh-Eichelberger-Rostoker (unsteady state PER) model[29]). V_{PL} is a characteristic plastic velocity representing the average velocity difference between the neighbouring jet segments [33]. The value of the characteristic plastic particle velocity is calculated by the same methodology in [2] after obtaining the necking strain at the specified average jet temperature due to jet heating.

4.5. Calculations of The Velocity Difference Between The Neighboring Jet Segments (V_{PL})

Starting from the general form for the Zerilli-Armstrong model; eq. (10) and applying Kolsky approach [34] and Walters and Summers [35], the characteristic plastic particle velocity V_{PL} is calculated accordingly using the stress-strain relation. Walters and Summers [35] obtained the the characteristic plastic particle velocity V_{PL} using Johnson-Cook, modified Johnson-Cook and Zerilli-Armstrong, at various temperatures for 75 μm copper grain size using the Kolsky model [34]. i.e.

$$V_{PL} = \frac{1}{\sqrt{\rho}} \int_0^{\varepsilon_N} \sqrt{\frac{d\sigma_e}{d\varepsilon_e}} d\varepsilon_e = \frac{1}{\sqrt{\rho}} \int_0^{\varepsilon_N} \sqrt{\frac{d\sigma}{d\varepsilon} - \sigma} d\varepsilon \quad (13)$$

Where, ε_N is the true strain achieved at the necking point, σ is the true plastic stress, ε is the true strain and ρ is the copper density; whereas subscript 'e' refers to engineering terms. This scheme was also used by Elshenawy and Li to calculate the VPL for shaped charges containing zirconium liners using the Johnson-Cook constitutive equation [14].

Following the same steps in ref. [35] and [34] and assuming constant jet and slug velocities during the stretching phase. Thus, the engineering strain-rate will then be considered independent of strain, or $d\dot{\epsilon}_e/d\varepsilon = 0$. In addition, the stretching process is simplified as to be an isothermal (i.e. $\frac{dT}{d\varepsilon} = 0$) as it happens during very short time interval [35]. Therefore, the derivative of Z-A Eq. (8) gives:

$$\frac{d\sigma}{d\varepsilon} = (C_1 e^{-C_2 T} \dot{\varepsilon}^{C_3 T} \varepsilon^{-0.5}) \left(\frac{1}{2} - C_3 T \varepsilon \right) \quad (14)$$

Because $\dot{\varepsilon} = \dot{\varepsilon}_e e^{-\varepsilon}$; thus

For the stability condition; $\frac{d\sigma}{d\varepsilon} = \sigma$, the necking strain (ε_N) can be calculated by:

$$(C_1 e^{-C_2 T} \dot{\varepsilon}^{C_3 T} \varepsilon^{-0.5}) \left(\frac{1}{2} - C_3 T \varepsilon \right) = C_1 \varepsilon^{0.5} e^{(-C_2 T + C_3 T \ln \varepsilon)} + C_4 + C_5 \quad (15)$$

After simplification and denoting ε by the necking strain ε_N ,

$$C_4 + \frac{C_5}{\sqrt{d}} + C_1 e^{-C_2 T} \dot{\varepsilon}^{C_3 T} \left(\sqrt{\varepsilon_N} - \left[\frac{0.5 - C_3 T \varepsilon_N}{\sqrt{\varepsilon_N}} \right] \right) = 0 \quad (16)$$

The true engineering strain rate is unknown, thus it will be replaced by $\dot{\varepsilon}_e e^{-\varepsilon}$. Eq (14) takes the form of:

$$\left(C_4 + \frac{C_5}{\sqrt{d}} \right) + C_1 e^{-C_2 T} (\dot{\varepsilon}_e)^{C_3 T} (e^{-\varepsilon_N C_3 T}) \left(\sqrt{\varepsilon_N} - \left[\frac{0.5 - C_3 T \varepsilon_N}{\sqrt{\varepsilon_N}} \right] \right) = 0 \quad (17)$$

The substitution of the ZA constants, Eq. (17) will be solved for the necking strain; ε_N . The true dynamic strain-rate $\dot{\varepsilon}$ in Eq. (17) can be estimated by:

$$V_{PL} = \frac{1}{\sqrt{\rho}} \int_0^{\varepsilon_N} \sqrt{\left(C_4 + \frac{C_5}{\sqrt{d}} + C_1 e^{-C_2 T} (\dot{\varepsilon}_e e^{-\varepsilon_N})^{C_3 T} \left(\sqrt{\varepsilon_N} - \left[\frac{0.5 - C_3 T \varepsilon_N}{\sqrt{\varepsilon_N}} \right] \right) \right)} d\varepsilon_N \quad (22)$$

$$V_{PL} = \frac{1}{\sqrt{\rho}} \int_0^{0.2876} \sqrt{\left(95 + 82.926 (2.025 \times 10^5)^{0.000115T} (e^{-\varepsilon_N})^{0.000115T} \left(\sqrt{\varepsilon_N} - \left[\frac{0.5 - 0.000115T \varepsilon_N}{\sqrt{\varepsilon_N}} \right] \right) \right)} d\varepsilon \quad (23)$$

The integration is performed using the area under the curve over the strain range from 0 to ε_N for each specified grain size and the calculated temperature generated from plastic deformation heating and for each average grain size. The plastic particle velocity will then be estimated after estimating the jet temperature numerically, which will be discussed in details in section 4.6.

$$\dot{\varepsilon} = \dot{\varepsilon}_e e^{-\varepsilon} \quad (18)$$

in which, $\dot{\varepsilon}_e$ is the initial engineering strain-rate of stretching jet that can be approximated by [35]:

$$\dot{\varepsilon}_e = \frac{V_o}{l_{eff}} \quad (19)$$

Where, l_{eff} is the effective jet length at the beginning of the stretching process and can be estimated by:

$$l_{eff} = l_s \frac{V_o - V_c}{V_o} \quad (20)$$

Where, l_s is the slant height of the liner. V_{tip} and V_{rear} are the jet tip and slug velocities; respectively. The total strain rate values are listed in Table 2. The calculated engineering strain rates were found to vary between 2.025×10^5 and 2.033×10^5 s⁻¹ for the range of the liner average grain sizes ranging from 10.63 μ m to 49.38 μ m; respectively. Hence, as an example; for the average grain size of 10.63 μ m; Eq. (17) take the form:

$$95 + 890 e^{-0.0028T} (2.025 \times 10^5)^{0.000115T} e^{-0.000115T \varepsilon_N} \left(\sqrt{\varepsilon_N} - \left[\frac{0.5 - 0.000115T \varepsilon_N}{\sqrt{\varepsilon_N}} \right] \right) = 0 \quad (21)$$

The maximum necking strain ε_N can then be estimated by solving Eq.(21), which was found to be 0.2876 and depends on the engineering strain-rate and the jet heating temperature for each average grain size of the copper material. Other necking strain values for the remaining grain sizes will be listed in Table 2.

Thus, the characteristic plastic particle velocity V_{PL} can be estimated using Eq. (13) depending on true stress and true strain as seen in Eq. (22) and its simplest form, Eq. (23), for the smallest grain size of 10.63 μ m.

4.6. The Jet Temperature Estimation

The jet temperature is very important in determining the plastic particle velocity (V_{PL}), so that it should be precisely predicted to make sure that the calculated necking strain is very close to the real one. In order to find the jet temperature during the stretching process, Autodyn was used by Agu[32] to simulate BRL-81.3 [36] shaped charge jet formation

depending on Mei-Gruneisen thermodynamic model, which considers the shock equation of state of the copper liner material. The measured average temperature that was measured and recorded and found 432oC with a standard deviation of 76oC by Von Holle and Trimble [37]. The jet temperature were measured at travelling distance of eight times of its diameter of 81.3mm. Agu[32] concluded that the jet temperature varies across the jet loop direction with the largest recorded temperature found near the jet axis, while the outer surface temperature ranges from 795K to 905K, which means validation of the used hydrocode and the used Mei-Gruneisen thermodynamic model in predicting the jet temperature. The same conclusion was observed by Elshenawy[38] who calculated the temperature for the same shaped charge jet and found the outer layer has a value of 780 K (i.e. 503°C), which also confirms the validity of the suggested hydrocode for temperature evaluation. Sample of the jet estimation model for the liner with grain size of 49.38 μm at time of 20.12 μs from the detonation moment is shown in Figure 6.

This figure shows the temperature distribution contours for a fixed Gauge point located on the outer surface of the jet material for the liner with grain size of 49.38 μm . The steady state temperature that was recorded for this grain size liner is 921K, whereas the smaller grain size liners exhibited lower jet temperatures. The range of this jet temperature heating over the entire liner average grain size is 39K, which represents only 4% out of the maximum obtained temperature for the 49.38 μm . The entire jet average temperatures for the entire grain sizes are shown in Table 2.

The estimated V_{PL} values in Table2 are then used to calculate the elemental breakup times for the studied jets using liners with different grain sizes as depicted in the same table.

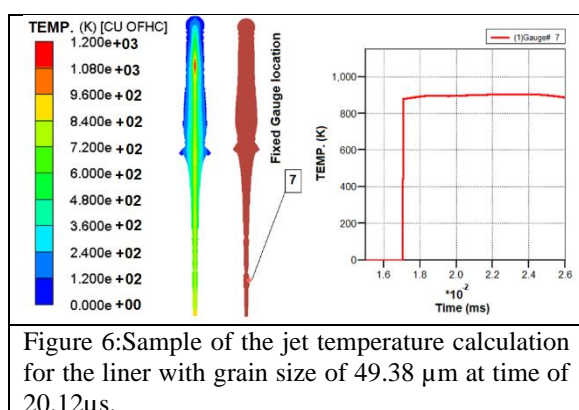


Figure 6: Sample of the jet temperature calculation for the liner with grain size of 49.38 μm at time of 20.12 μs .

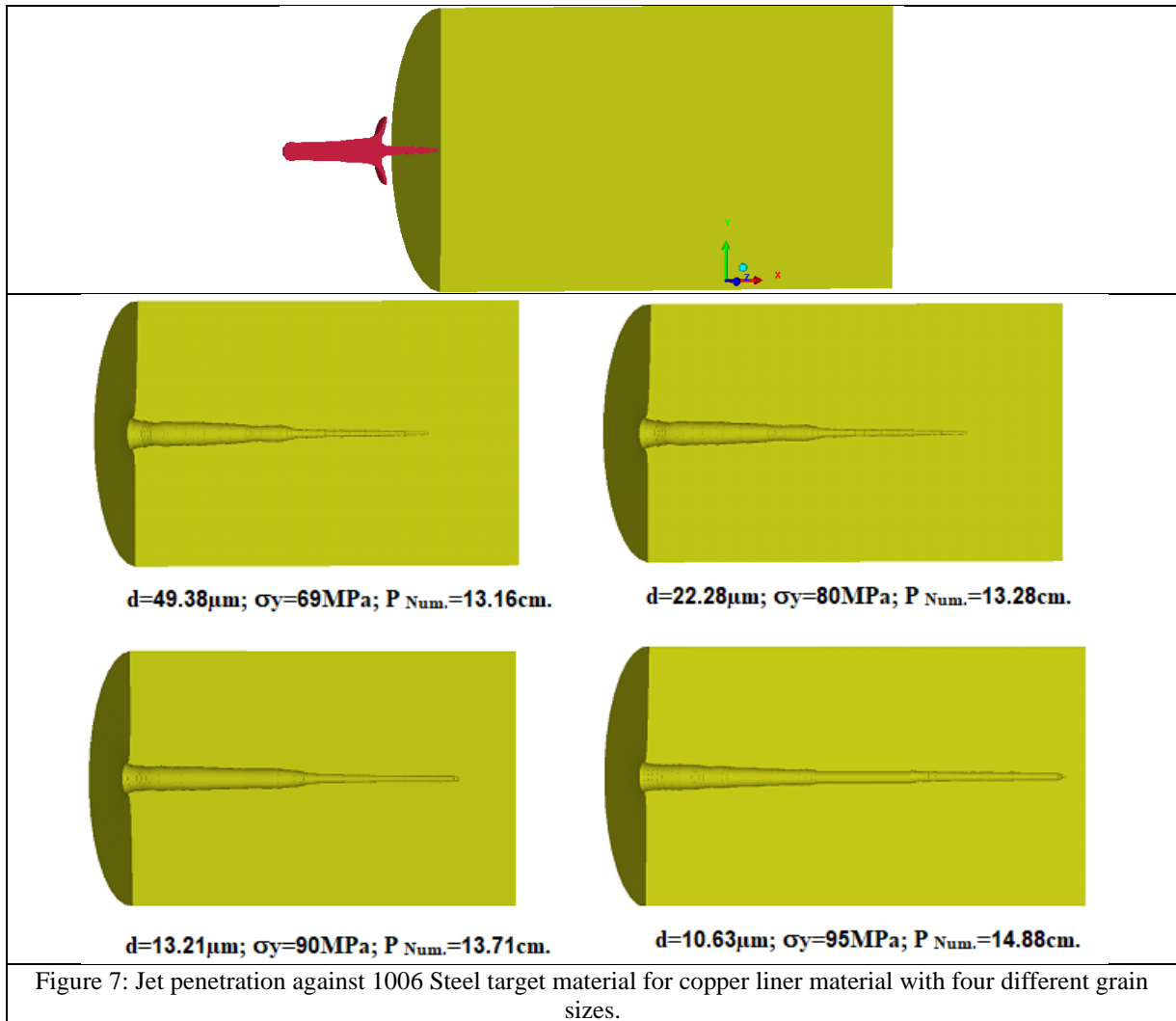
The calculated breakup time for the four jets having different grain sizes exhibits an inverse relationship with the initial liner grain size, which is similar to the extensive calculations over wide range of copper liners [2]. This may be clarified by the variation in the penetration evaluation analytically, when this breakup time shows significant effect within penetration section.

4.7. Jet Penetration:

The penetration potentials of the copper jets having different grain sizes and relevant yield strength values are performed numerically against 1006 steel target material using copper liner materials with four different grain sizes of 49.38, 22.27, 13.21 and 10.62 μm corresponding to yield strength values of 69, 80, 90 and 95 MPa; respectively as shown in Figure 7. The copper with grain size value of 49.38 μm was obtained using various stages of heat treatments prior to plastic deformation and cold working of the copper discs. This value is necessary to extend and cover wide ranges of both grain size and relevant yield strength values. Other grain size values ranging from 10.62 to 22.27 were obtained by the normal annealing cycles at temperatures 200 to 600°C as per Figure 3.

Since the erosion strain is crucial in determining the penetration depth numerically [17, 39, 40], it should be quantified within Lagrangian jet-target interaction. The erosion strain does not represent a physical parameter, but it represents a numerical algorithm, by which the mesh degeneracy (overlap) is discarded [17]. The erosion strain for the jet sub-grid is fixed at a value of 500% (i.e. erosion strain 5) whereas the steel 1006 has various an incremental erosion strain values ranging from 0.1 to 0.5. The purpose of these iterations is to find out the best values of the erosion strain values, at which the numerical penetration becomes close to the real experiment as much as possible. It was found that increasing the erosion strain values from 0.1 to 0.5 will decrease the achieved penetration depth of the jet into steel 1006 targets. The five polynomial curves seem to converge at erosion strain value of 0.5, with an overall maximum error of 4% when compared to the experimental one.

Based on data obtained from figure 7, it can be concluded that smaller copper grain size yields larger penetration depth and vice versa for both the experimental field testing and the numerical calculations. The same fact was emphasized by the static firing test performed using liners with the same different grain sizes as shown in Figure 8.



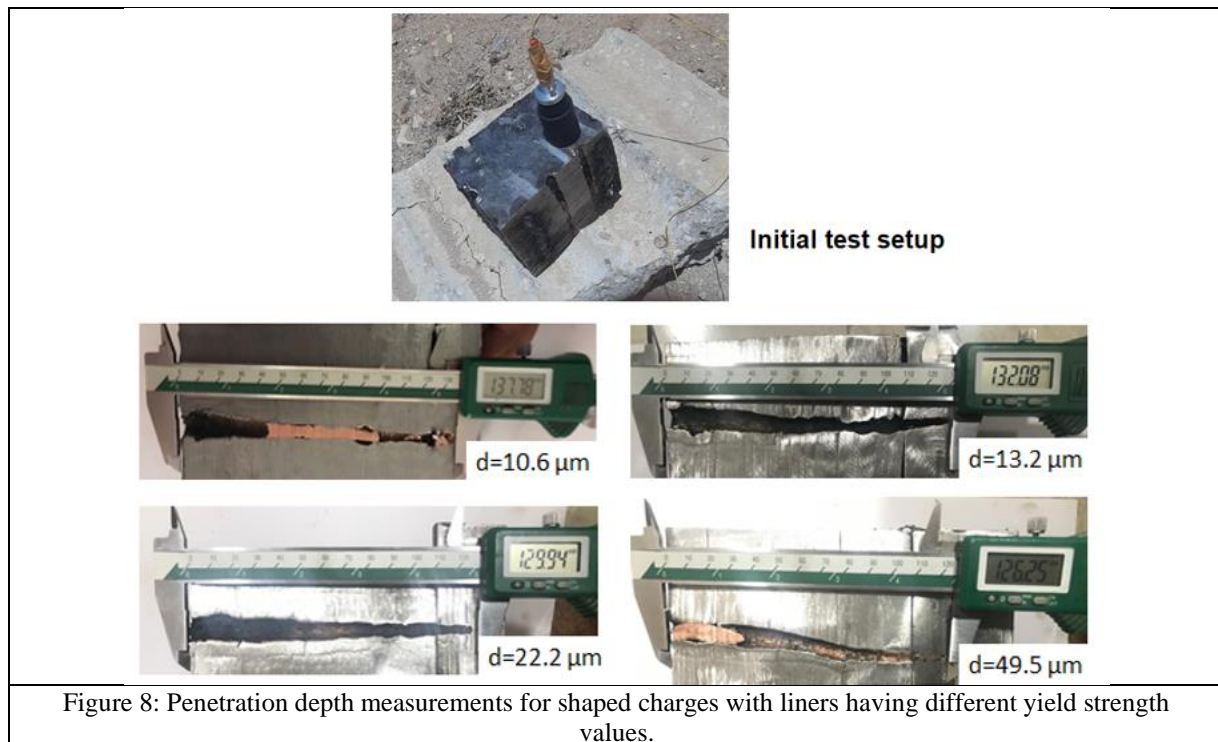


Figure 8: Penetration depth measurements for shaped charges with liners having different yield strength values.

The penetration-average grain size can be described by inverse linear relationship even though the slight variation in this relation, it cannot be ignored but should be considered. The same phenomenon is common in both experimental and numerical estimates. The reason behind this relation may be attributed to the breakup time and the effective jet length prior to fragmentation, which seems to be higher for liners with fine grain sizes. Another reason may be concluded from Table 3 using analytical models. In this table, the numerical estimates; V_o , V_c are obtained from jet formation and penetration models respectively; the effective jet length (Z_o) is obtained numerically using the same approach in ref. [39] and verified using the jetting analysis and relevant scheme [40]. Unfortunately, the analytical penetration model shown in Eq. (4) cannot be used directly in the current form because the modification (i.e. Eq. (4)) does not consider the variation in the yield strength of the jet material when the liner average grain size regarded. Thus, when only one target material is used with different grain size liners, another reduction term based on Equations (3:5) can be introduced, in which the dynamic yield strength of the target in Eq. (2) and the compression strength of concrete in Eq. (3) and the target yield strength in Eq. (4) are replaced by the resistance to plastic deformation; i.e. $\sigma = \sigma_T - \sigma_j$, Eq. (1). Therefore, the suggested reduction term may take the form:

$$\left(1 - \lambda \frac{\sigma_T - \sigma_j}{\rho_j V_c^2}\right) \quad (24)$$

while the resistance to plastic deformation is represented by three times to the uniaxial yield strength values of both the target and jet materials; respectively [11, 12].

By combining the approach used in Ref. [20] and the suggested correction term Eq. (24) is added to case (b) in Allison and Vitalli model [16] (break-up during penetration in our shaped charge because it is the most common scenario), an analytical modified penetration equation can be suggested as follow:

$$P = \left(\frac{(y+1)(V_o t_b)^{\frac{1}{y+1}} Z_o^{\frac{y}{y+1}} - V_c t_b}{r} - Z_o \right) \left(1 - \lambda \frac{\sigma_T - \sigma_j}{\rho_j V_c^2} \right) \quad (25)$$

This equation will be used to calculate the penetration depth when the jet yield strength is taken into account as shown in Table 3.

Data summarized in Table (3) was used to represent the penetration-average grain size dependence in accordance with Figure 9. P-ideal, which refers to analytical penetration without correction term that cannot be used to describe penetration depth when various grain sizes liners are tested and maintaining the same testing conditions. The modified model based on target and liner yield

strength correction shown in Eq. (25) is valid over the studied wide range of grain size from 10 μm up to the maximum studied grain size of 49 μm with reasonable accepted error of only 1.8%, which confirms the validity of the proposed model over this grain size

range (i.e. 10: 49 μm) with satisfactory predicted results.

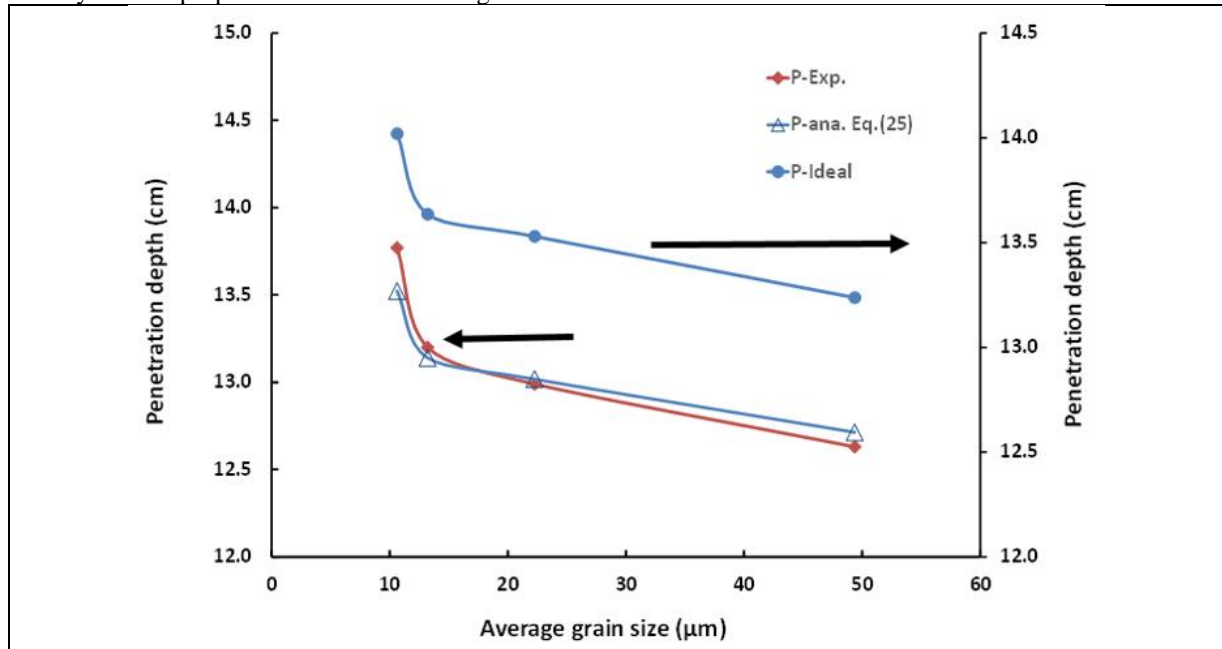


Figure 9: The ideal (non-corrected), experimental and corrected DoP for liners with different average grain sizes.

The longest breakup time, the lowest cut-off velocity and the largest effective jet length (Z_0) are the main reasons why the finest grain size liner exhibits the largest penetration depth into steel target material. This confirms the feasibility of the heat treatment study and its impact on the relevant properties of produced grain size and mechanical properties [41-43]. Although the analytical calculations showed the largest error of 1.8% at the smallest grain size when

compared to the experimental test, but the other three charges showed satisfactory results with only maximum absolute error of 0.66 %. Eventually, the bottom line is this, in order to enhance the penetration capability of a shaped charge C10100 copper liner, some requirements of liner material has to be met and the liner average grain size and its microstructure are on the top of these requirements.

Table 1: Ultimate, yield strengths and elongation for the copper liners annealed at different temperatures for 30 minutes.

Sample	Annealing Temperature ($^{\circ}\text{C}$)	σ_y (Mpa)	σ_u (Mpa)
0	Cold worked	152	260.42
A	200	91	237.58
B	250	85	227.01
C	300	81	224.69
D	350	76	219.31
E	400	72	218.57
F	450	70	215.41
G	500	68	211.79
H	550	64	211.71
I	600	62	208.05

Table 2: The necking strain and the characteristic plastic particle velocity V_{PL} for a shaped charge with different grain sizes.

Liner average grain size (μm)	10.63	13.21	22.28	49.38
V_o (m/s)	8280	8285	8294	8302
V_c (m/s)	1238	1240	1246	1250
l_s	48.07	48.07	48.07	48.07
l_{eff} ; Eq. (20) (mm)	40.88	40.88	40.88	40.88
$\dot{\epsilon}_e$ (s^{-1}) Eq. (19)	2.025×10^5	2.027×10^5	2.030×10^5	2.033×10^5
Jet average temperature (K)	882	903	911	921
Necking strain ϵ_N (-)	0.2876	0.2902	0.3031	0.3179
V_{PL} ; Eq. (22) (m/s)	96.08	97.81	98.31	99.69
Jet radius Eq. (12) (mm)	1.73	1.71	1.70	1.69
Breakup time; Eq. (11) (μs)	36.0	35.0	34.5	34.0

Table 3: The jet characteristics and the penetration calculation parameters for the liners with different grain sizes.

Liner average grain size (μm)	10.63	13.21	22.28	49.38
Liner yield strength (MPa)	95.0	90.0	80.0	69.0
Target yield strength (MPa)	285	285	285	285
ρ_T (kg/m^3)	7800	7800	7800	7800
ρ_j (kg/m^3)	8900	8900	8900	8900
γ (-)	0.94	0.94	0.94	0.94
Z_o (mm)	37.0	36.0	36.0	35.0
V_o (m/s)	8280	8285	8294	8302
V_c (m/s)	1238	1240	1246	1250
t_b (ms)	0.0360	0.0350	0.0345	0.0340
P-ideal ^a (cm)	14.02	13.64	13.53	13.24
$(\sigma_T - \sigma_j)/\rho_j V_c^2$	0.0418	0.0427	0.0445	0.0466
λ calculated; Eq.(6)	0.849	0.849	0.849	0.849
P-ana ^b Eq.(25) (cm)	13.52	13.14	13.02	12.71
P-Exp. ^c (cm)	13.77	13.20	12.99	12.63
Error ^d (%)	1.80	0.45	-0.22	-0.66

P-ideal^a : ideal penetration calculated by Eq.(25) without correction term.

P-ana^b: the penetration depth using Eq.(25) considering target and jet yield strengths and correction term.

P-Exp.^c experimental penetration

Error^d%=(P-Exp.- P-ana Eq.(25) / P-Exp.) \times 100

5. Conclusions

Based on mechanical testing of annealed C10100 copper used as shaped charge liners with different grain size and relevant mechanical properties, some findings can be obtained as follow:

- The annealing temperature of the cold worked C10100 copper liners was found to have significant effects on the produced grain size, the material hardness and the relevant mechanical properties, which in turn are related directly to its jet breakup time and penetration capability into 1006 steel targets.

In addition, Allison & Vitalli formula of jet penetration prediction is modified based on numerical and experimental testing to include resistance to plastic deformation, which considers both target and liner yield strengths values (i.e. three times yield strength value). The suggested correction term was found valid from 10 μm grain size up to 49 μm to give reasonable accepted values when compared to experimental test with maximum absolute error of 1.8% when compared to experimental field testing.

- The impact of the liner average grain size and the corresponding yield strength has been addressed numerically, where the jet with fine grain size and higher yield strength produces slower jet than that with coarse grains.
- Little variation in the calculated average jet temperature was concluded for the fine grain size of 10.63 μm , which showed 882K and 921K for the coarse grain size liner of 49.38 μm .
- The velocity difference between two neighboring jet segments (VPL) showed little variation between 96.08 and 99.69 m/s for the copper liner with grain sizes ranging from 10.63 to 49.38 μm ; respectively.
- The increase in the annealing temperature of the C10100 copper by 20.8oC decreases the Vicker's hardness by 1 HV.
- The grain size of the C10100 copper increases by 1 μm with every 28oC increase in the annealing temperature under controlled atmosphere.

6. Conflicts of interest

The authors declare that they have no known competing financial interests or personal relationships that could have appeared to influence the work reported in this paper. "There are no conflicts to declare".

7. Formatting of funding sources

The authors would like to thank the Egyptian Armed forces for helping achieve these experiments and withdraw these conclusions.

8. Acknowledgments : The authors would like to thank the Egyptian Armed forces for helping achieve these experiments and withdraw these conclusions.

9. References

- [1] X. Li, M. Xu, J. Wang, H. Xu. Study on grain refinement of copper-based liner by vacuum gradient heat treatment process using response surface methodology. *J. Mater. Res. Technol.*, **2021**, vol. 15, p. 2345–2354. DOI: [10.1016/j.jmrt.2021.09.066](https://doi.org/10.1016/j.jmrt.2021.09.066).
- [2] T. Elshenawy. Determination of the velocity difference between Jet Fragments for a range of copper liners with different small grain sizes. *Propellants, Explos. Pyrotech.*, **2016**, vol. 41, no. 1, p. 69–75. DOI: [10.1002/prep.201500095](https://doi.org/10.1002/prep.201500095).
- [3] F. J. Zerilli, R. W. Armstrong. Constitutive relations for the plastic deformation of metals. *AIP conference proceedings*. **1994**, Vol. 309. No. 1. American Institute of Physics, p. 989-992. DOI: [10.1063/1.46201](https://doi.org/10.1063/1.46201).
- [4] J. Petit, V. Jeanclaude, C. Fressengeas. Effects of liner grain size on shaped - Charge jet performance: A combined experimental/numerical/analytical approach. *J. Phys. IV JP*, **2006**, vol. 134p. 379–384. DOI: [10.1051/jp4:2006134058](https://doi.org/10.1051/jp4:2006134058).
- [5] J. Ridhwan, M. Syafiq, M. H. M. Hafidzal, M. S. Zakaria, and M. A. M. Daud. Effect of cooling rate on microstructures and mechanical properties of C102 copper alloy. *J. Mech. Eng. Technol.*, **2014**, vol. 6, no. 1, p. 87–94. [Online]. Available: <https://journal.utem.edu.my/index.php/jmet/article/view/345>
- [6] Edwards, M., Mustey, and A., Young, R. The effect of liner mechanical properties on the pweformance of copper explosively formed projectiles. In *European Forum on Ballistics of Projectilies*, **2000**, p. 435. [Online]. Available: <https://apps.dtic.mil/sti/pdfs/ADA385710.pdf#page=419>
- [7] M. A. Meyers, U. R. Andrade, and A. H. Chokshi. The effect of grain size on the high-strain, high-strain-rate behavior of copper. *Metall. Mater. Trans. A*, **1995**, vol. 26, no. 11, p. 2881–2893. DOI: [10.1007/BF02669646](https://doi.org/10.1007/BF02669646).
- [8] A. J. Schwartz, M. Kumar, D. H. Lassila. Analysis of intergranular impurity concentration and the effects on the ductility of copper-shaped charge jets. *Metall. Mater. Trans. A Phys. Metall. Mater. Sci.*, **2004**, vol. 35 A, no. 9, p. 2567–2573. DOI: [10.1007/s11661-004-0203-8](https://doi.org/10.1007/s11661-004-0203-8).
- [9] H. O. Agu, A. Hameed, G. J. Appleby-Thomas. Comparison of the microstructure of machined and laser sintered shaped charge liner in the hydrodynamic regime. *J. Dyn. Behav. Mater.*, **2019**, vol. 5, no. 4, p. 484–494. DOI: [10.1007/s40870-019-00213-y](https://doi.org/10.1007/s40870-019-00213-y).
- [10] W. H. Tian, A. L. Fan, H. Y. Gao, J. Luo, and Z. Wang. Comparison of microstructures in electroformed copper liners of shaped charges before and after plastic deformation at different strain rates. *Mater. Sci. Eng. A, Jun*, **2003**, vol. 350, no. 1–2, p. 160–167. DOI: [10.1016/S0921-5093\(02\)00721-9](https://doi.org/10.1016/S0921-5093(02)00721-9).
- [11] R. J. Eichelberger. Re-examination of the nonsteady theory of jet formation by lined cavity charges. *J. Appl. Phys.*, **1955**, vol. 26, no. 4, p. 398–402. DOI: [10.1063/1.1722005](https://doi.org/10.1063/1.1722005).
- [12] R. J. Eichelberger. Experimental test of the theory

- of penetration by metallic jets. *J. Appl. Phys.*, **1956**. vol. 27, no. 1, p. 63–68. DOI: [10.1063/1.1722198](https://doi.org/10.1063/1.1722198).
- [13] D. C. Pack, W. M. Evans. Penetration by high-velocity (munroe) jets: I. *Proc. Phys. Soc. Sect. B*, Apr. **1951**. vol. 64, no. 4, p. 298. DOI: [10.1088/0370-1301/64/4/302](https://doi.org/10.1088/0370-1301/64/4/302).
- [14] W. Johnson, N. Jones. Appreciations of professor william (bill) johnson. *Int. J. Impact Eng.*, **2011**. vol. 38, no. 5, p. 265–274. DOI: [10.1016/j.ijimpeng.2011.02.007](https://doi.org/10.1016/j.ijimpeng.2011.02.007).
- [15] A. A. Wells. Impact Strength of Materials. *Int. Metall. Rev.*, **1972**. vol. 1, no. 1, p. 264–265. DOI: [10.1179/imtr.1972.17.1.264](https://doi.org/10.1179/imtr.1972.17.1.264).
- [16] Allison, F. E. , Raffaella Vitali. A New method of computing penetration variables for shaped-charge jets, **1963**. [Online]. Available: <https://apps.dtic.mil/sti/citations/AD0400485>
- [17] T. Elshenawy, Q. M. Li. Influences of target strength and confinement on the penetration depth of an oil well perforator. *Int. J. Impact Eng.*, April **2013**. vol. 54, no. p. 130–137 DOI: [10.1016/j.ijimpeng.2012.10.010](https://doi.org/10.1016/j.ijimpeng.2012.10.010).
- [18] Q. M. Li, H. Meng. About the dynamic strength enhancement of concrete-like materials in a split Hopkinson pressure bar test. *Int. J. Solids Struct.*, Jan. **2003**. vol. 40, no. 2, p. 343–360. DOI: [10.1016/S0020-7683\(02\)00526-7](https://doi.org/10.1016/S0020-7683(02)00526-7).
- [19] B. Grove, J. Heiland, I. Walton. Geologic materials' response to shaped charge penetration. *International Journal of Impact Engineering*, **2008**. Volume 35, Issue 12, P. 1563-1566. <https://www.sciencedirect.com/science/article/pii/S0734743X08001656>
- [20] T. Elshenawy, A. Elbeih, Q. M. Li. Influence of target strength on the penetration depth of shaped charge jets into RHA targets. *Int. J. Mech. Sci.*, **2018**. vol. 136, p. 234–242 DOI: [10.1016/j.ijmecsci.2017.12.041](https://doi.org/10.1016/j.ijmecsci.2017.12.041).
- [21] T. W. Wright, Frank, T.W.a.C. BRL Report BRL-TR-2957, 1988.
- [22] Z. Rosenberg and E. Dekel. A critical examination of the modified Bernoulli equation using two-dimensional simulations of long rod penetrators. *Int. J. Impact Eng.*, **1994**. vol. 15, no. 5, p. 711–720 DOI: [10.1016/0734-743X\(94\)90199-U](https://doi.org/10.1016/0734-743X(94)90199-U).
- [23] Y. Partom, C.E.A., Jr., D.L. Orphal. Revisiting RT in Proc. 18th Int. Symp. Ballistics, **1999**, San Antonio, TX.
- [24] A. Doig. *Military Metallurgy.*, **2020**. DOI: [10.1201/9781003059400](https://doi.org/10.1201/9781003059400).
- [25] A. Interanational. Standard Guide for Preparation of Metallographic Specimens Standard Guide for Preparation of Metallographic Specimens 1. *ASTM Int.*, **2012**. vol. 03.01, no. July, p. 1–12. DOI: [10.1520/E0003-11R17.1](https://doi.org/10.1520/E0003-11R17.1).
- [26] G. Bi et al. Evaluation of uncertainty in determining average grain size by ASTM E112 standard. *IOP Conf. Ser. Mater. Sci. Eng.*, **2020**. vol. 733, no. 1. DOI: [10.1088/1757-899X/733/1/012045](https://doi.org/10.1088/1757-899X/733/1/012045).
- [27] ASTM, E8/E8M-22. Standard test methods for tension testing of metallic materials, **2022**. DOI: [10.1520/E0008_E0008M-22](https://doi.org/10.1520/E0008_E0008M-22)
- [28] International, A., A.S.f. Testing, and M.C.E.-o.M. Testing, Standard Test Methods for Tension Testing of Metallic Materials. *ASTM International*.
- [29] E. M. Pugh, R. J. Eichelberger, N. Rostoker. Theory of jet formation by charges with lined conical cavities. *J. Appl. Phys.* **1952**. vol. 23, no. 5, p. 532–536. DOI: [10.1063/1.1702246](https://doi.org/10.1063/1.1702246).
- [30] V. Y. Gertsman, M. Hoffmann, H. Gleiter, R. Birringer. The study of grain size dependence of yield stress of copper for a wide grain size range. *Acta Metall. Mater.*, **1994**. vol.42, no.10, pp. 3539–3544. DOI: [10.1016/0956-7151\(94\)90486-3](https://doi.org/10.1016/0956-7151(94)90486-3).
- [31] B. Bourne, K. G. Cowan, J. P. Curtis. Shaped charge warheads containing low melt energy metal liners. *Proc. 19th Int. Symp. Ballist.*, **2001**.no. May, p. 583–590, [Online]. Available: http://www.ciar.org/ttk/mbt/papers/symp_19/WM05_583.pdf
- [32] H. Agu. The effect of 3D printed material properties on shaped charge liner performance, **2019**, [Online]. Available: <https://ethos.bl.uk/OrderDetails.do?uin=uk.bl.ethos.802240>.
- [33] Hirsch scaling Hirsch, E., *Scaling of the Shaped Charge Jet Break Up Time*. *Propellants, Explosives, Pyrotechnics*, **2006**. **31**(3): p. 230-233. DOI: [10.1002/prop.200600031](https://doi.org/10.1002/prop.200600031)
- [34] Kolsky, H., *Stress waves in solids Unabridged republication ed.* **1963**. DOI: [10.1016/0022-460X\(64\)90008-2](https://doi.org/10.1016/0022-460X(64)90008-2)
- [35] Walters, W.P., *The Velocity Difference Between Particulated Shaped Charge Jet Particles for Face-Centered-Cubic Liner Materials*. **1992**, DTIC Document. [Online]. Available: <https://apps.dtic.mil/sti/citations/ADA257348>.
- [36] Aseltine, C.L., *Analytical Predictions of the Effect of Warhead Asymmetries on Shaped Charge Jets*. **1980**, DTIC Document. [Online]. Available: <https://apps.dtic.mil/sti/citations/ADA083437>
- [37] Von Holle, W. and J. Trimble, Temperature measurement of shocked copper plates and shaped charge jets by two color ir radiometry. *Journal of Applied Physics*, **1976**. 47(6): p. 2391-2394. DOI: [10.1063/1.323028](https://doi.org/10.1063/1.323028)
- [38] Elshenawy, T. and Q.M. Li, Breakup Time of Zirconium Shaped Charge Jet. *Propellants, Explosives, Pyrotechnics*, **2013**. 38(5): p. 703-708. DOI: [10.1002/prop.201200191](https://doi.org/10.1002/prop.201200191)

-
- [39] Elshenawy, T.; Elbeih, A.; Klapötke, T.M. A Numerical Method for the Determination of the Virtual Origin Point of Shaped Charge Jets Instead of Using Flash X-ray Radiography. *J. Energ. Mater.* **2018**, *36*(2): p.127-140. DOI: [10.1080/07370652.2017.1324532](https://doi.org/10.1080/07370652.2017.1324532)
- [40] Agu, H.O., A. Hameed, and G. Appleby-Thomas, Application of shell jetting analysis to determine the location of the virtual origin in shaped charges. *International Journal of Impact Engineering*, **2018**, *122*: p. 175-181. DOI: [10.1016/j.ijimpeng.2018.04.014](https://doi.org/10.1016/j.ijimpeng.2018.04.014)
- [41] Jin K, Qi L, Kang H, Wang W, Guo Y, Li Y. The Yield Behavior of Oxygen-Free Copper Under Biaxial Quasi-Static and Dynamic Loadings. **2023**. Available at: [SSRN 4384128](https://ssrn.com/abstract=4384128).
- [42] Jin K, Qi L, Kang H, Guo Y, Li Y. A novel technique to measure the biaxial properties of materials at high strain rates by electromagnetic Hopkinson bar system. *International Journal of Impact Engineering*. **2022**. Sep 1;167:104286. DOI: [10.1016/j.ijimpeng.2022.104286](https://doi.org/10.1016/j.ijimpeng.2022.104286)
- [43] Cañadilla A, Romero A, Rodríguez GP, Caminero MÁ, Dura ÓJ. Mechanical, Electrical, and Thermal Characterization of Pure Copper Parts Manufactured via Material Extrusion Additive Manufacturing. *Materials*. **2022** Jul 1;15(13):4644. DOI: [10.3390/ma15134644](https://doi.org/10.3390/ma15134644)